Integration of Monte-Carlo particle transport Simulations Into a TCAD Workflow

Olivier Marcelot
ISAE-SUPAERO
Toulouse, France
o.marcelot@isae.fr

Damien Lambert
CEA-DAM
Arpajon, France
ORCID 0000-0003-2150-4315

***Abstract*—A new methodology is presented with the aim to directly include Geant4 outputs into a TCAD workflow. With such a method, it is now possible to fully simulate a particle detector in the TCAD workflow with variations of electric field, potentials, induced by a timing diagram applied to a pixel, together with a full particle distribution.**

***Index Terms*—Numerical simulation, Monte Carlo methods, Particle beams, Semiconductor detectors.**

I. Introduction

CMOS particle detectors are largely used for scientific applications, such as in electron microscopy [1], particle detection at the CERN experiment [2], are even in medical applications as for instance the PET-scan [3]. Thanks to multiple improvements in performances and especially in the radiation hardness, CMOS sensors are commonly employed and are still actively developed for these applications. Currently, such devices can be studied by means of a Technology Computer Aided Design (TCAD) software, similarly to other semiconductor devices, the goal being to improve the understanding of the device under test and to reduce the amount of prototype variations to be developed and tested.

However, major TCAD softwares do not propose any native solution for the simulation of particles such as electrons or protons. Indeed, these softwares only propose models for optical generations, or a basic heavy ion and Alpha particle model [4]. Nowadays, results of the Geant4 particle transport simulator can be adapted to calibrate heavy ion or alpha particles TCAD parameters [5]–[7], or TCAD simulations can be combined with a particle simulator output to a third party simulator such as the Allpix framework [2], [8], [9]. With the first method, an additional calibration step is needed and does not guaranty the good matching between the TCAD heavy ion or alpha model and Geant4, moreover this calibration must be done each time the particle beam is modified. In addition, particle Monte Carlo modeling can give an accurate volume deposition for each particle tracks, where as analytical formula can give an average value of the deposition. In the latter method, the main drawback is the fact that the particle distribution cannot be simulated in the TCAD workflow, avoiding the simulation of bias variations, gate operations, together with the particle distributions and usage of eventual timing diagram. Another drawback is the use of an additional third party simulator.

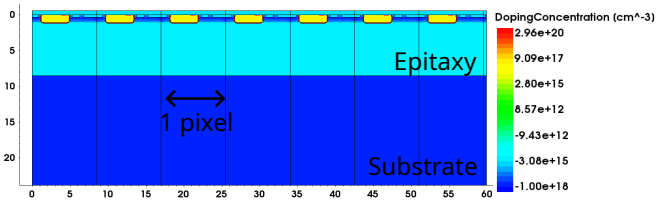

Fig. 1. TCAD 2 dimensional simulation of the doping concentration of 7 pixels in cross-section.

Therefore, for both solution, the developed pixel cannot be precisely simulated with all parameters.

To overcome these issues, a new methodology is proposed in this work in order to efficiently and quickly integrate the Geant4 Monte-Carlo outputs within the Synopsys Sentaurus workbench. To do so, the positions of all particles simulated with Geant4 are converted into an optical generation data usable by the TCAD software. The methodology is presented and then limitations are discussed. This work is based on a similar process already presented for the Casino Monte Carlo program [10], but extended to Geant4 with a more complex structure.

II. Methodology

The Synopsys Sentaurus TCAD software 2020-09 is used in this work, and several 3T (3 transistors) pixels are simulated for the demonstration. The pixel has a $8.5\ \mu\mathrm{m}$ pitch and includes a conventional photodiode. It is designed on a $7\ \mu\mathrm{m}$ silicon epitaxy doped at $10^{15}\ \mathrm{boron/cm^3}$ resting on a more doped substrate and 7 identical pixels are simulated is order to include all the particle distribution, as shown by the Fig. 1. A top oxide is also added, similarly to the one used to isolate inter-connexion layers.

For the study, a Geant4 simulation [11]–[13] of electron particles is performed and is integrated in the Sentaurus environment. For this purpose, 100 electrons are accelerated at 200 kV and hit the device defined in Geant4 as in the following:

- silicon substrate with dimensions $200 \times 200 \times 200\ \mu\mathrm{m}^3$
- $5\ \mu\mathrm{m}$ of top-oxide on the silicon substrate, similarly to the one designed in the TCAD structure.

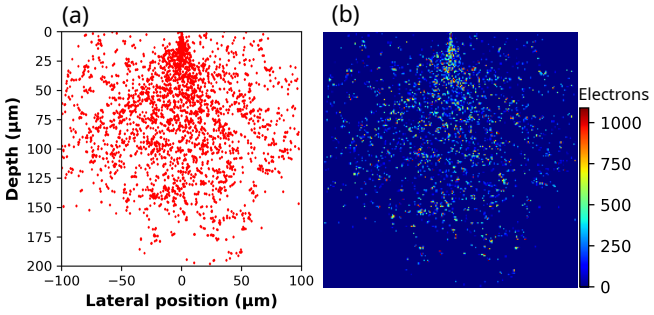

Fig. 2. (a) Geant4 simulation of 200 electrons at 200 kV in a silicon substrate. (b) Intermediate picture with a 500 nm mesh.

Fig. 3. Overview of the Geant4 conversion integrated in the Sentaurus workflow.

The model *em livermore* is activated and all electron collisions and secondary generations are recorded thanks to their coordinates and the energy loss. The output file is treated with a Python program in order to extract all remaining primary and secondary electron positions (Fig. 2 (a)).

In order to convert all particle coordinates into an optical generation file, the process is performed in two steps by means of a Python code:

- creation of an intermediate picture with a uniform mesh, where each point contains a number of generated electrons at the grid point
- read the Sentaurus grid file, and for each grid point interpolate the expected number of generated electrons from the intermediate picture.

Before doing this treatment the Sentaurus grid file must be converted into DF-ISE files in order to be readable in an external editor. This step is performed with the Sentaurus TDX tool. Therefore the whole process can be integrated in the Sentaurus workbench (Fig. 3).

The intermediate picture has a uniform mesh which is in the range of the largest Sentaurus mesh in the epitaxy region. For each particle, a script calculates the intermediate picture coordinate and the picture element is incremented accordingly. Finally a picture is obtained such as in Fig. 2 (b). At the end, the picture array is multiplied by an optical generation factor with the aim of approaching the requested carrier generation number in the Sentaurus device simulation. Indeed, the optical generation in Sentaurus in given in $\mathrm{cm}^{-3}\mathrm{s}^{-1}$ so the numbers in the intermediate picture in electrons need to be converted and also adapted with the expected number of incoming electrons during the integration time. The uniform mesh simplifies the process and if taken in the range of several 100 nm, it is supposed that it does not disturb the optical generation conversion. This aspect will be studied and discussed later. The whole conversion is performed in two steps because

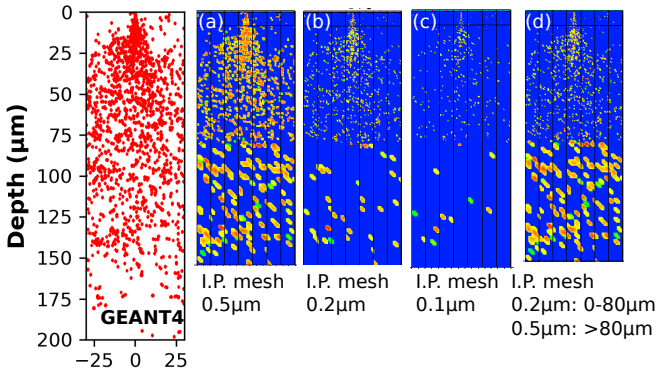

Fig. 4. Comparison between the Geant4 output and four optical generation in Sentaurus. (a), (b) and (c) are based on a unique intermediate picture (I.P.) mesh, while (d) on two I. P. meshes.

scanning all particle coordinates for each Sentaurus grid point would require a much longer process time. Indeed, with the proposed method, the particle coordinates are scanned only once, then the script directly reads the interpolated value in the intermediate picture at the requested coordinate.

The second script takes the Sentaurus *dat* file and read all region names where the optical generation should be created, as suggested by the work of Kelzenberg for a Lumerical to Sentaurus conversion [14]. Then, an array with identical dimensions compared to the intermediate picture is created and contains the coordinates of all picture elements given in nm. Finally, for every Sentaurus grid coordinate, the optical generation is interpolated from the values of the intermediate picture at the surrounded coordinates. The *dat* file is re-written with the optical generation data and the file converted in *tdr* format. With such a process, the optical generation file is created and an example is displayed in Fig. 4.

III. Validation of the Methodology

The Fig. 4 is showing a comparison between the Geant4 output and the Sentaurus optical generation for three intermediate picture meshes (a), (b) and (c), and for the same structure dimension given by the 7 pixels of the Fig. 1. As can be seen, a small intermediate picture mesh such as 200 nm may lead to missing particles as the Sentaurus grid points are more spaced than the intermediate picture ones and therefore some data of the intermediate picture are not read. Indeed, in the substrate at a depth higher than 80 μm the mesh resolution is 2 μm for reducing the computation time. On the other side, a larger mesh gives a better conversion of the particle position on the bulk substrate while the area near the surface and therefore with a much smaller Sentaurus mesh gives more approximate particle positions (picture (a)). An additional picture (Fig. 4 (d)) is showing the optical generation obtained with two intermediate picture meshes, a mesh of 200 nm between 0 and 80 μm, and a mesh of 500 nm from 80 μm. A much better situation is visible in this case at it combines a good resolution near the surface and much less missing particle in the deep substrate.

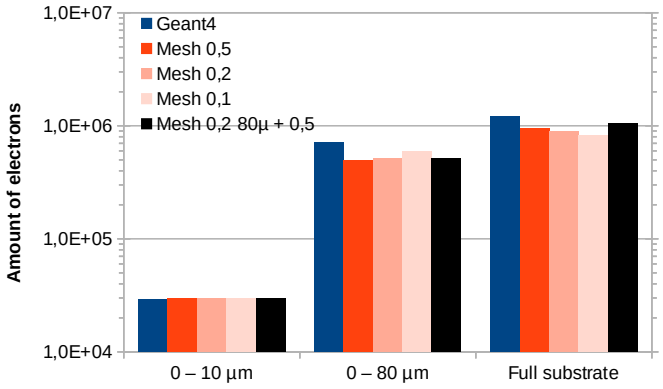

Fig. 5. Comparison of generated electrons in the substrate given by the Geant4 simulation for 30 incoming electrons at 200 kV, and by Sentaurus for four kinds of mesh grids in the intermediate picture: a unique 100 nm, 200 nm and 500 nm; and a combination of two mesh grids of 200 kV and 500 kV separated at 80 μm. The integration time is fixed at 1 μs, and the optical generation factor has been adapted in Sentaurus for the three variations in order to approximately match the Casino result. The full substrate is 500 μm thick.

In order to quantitatively compare the particles generated in Sentaurus and the ones generated by Geant4, the amount of generated electrons is estimated in a Sdevice simulation at various substrate thicknesses and is compared to the Geant4 output. For this purpose, an Sdevice simulation is run with all biases fixed at 0 V as only the optical generated carriers is monitored. An integration time of 1 μs is used, and an optical generation factor of 3×10^{19} cm^{-3}.s^{-1} is chosen in order to match with the Geant4 output. The amount of optically generated electrons is monitored in three regions of the substrate defined as in the following:

- from the surface to 10 μm depth: region with the smallest mesh in Sentaurus
- from the surface to 80 μm depth: region including the area with a mesh of 0.5 μm in Sentaurus
- all the substrate: in addition to the previous one it includes the area with a mesh of 2 μm

This exercise is performed for three unique intermediate picture meshes of 500 nm, 200 nm and 100 nm, and for a combination of two intermediate picture meshes of 200 nm and 500 nm separated at a depth of 80 μm.

The results are displayed in Fig. 5. As can be seen, near the surface and until 10 μm, the amount of electrons is quite well converted in Sentaurus, whatever the intermediate picture mesh. However, until a depth of 80 μm, the four configurations miss particles as the Sentaurus resolution is slightly larger than the intermediate picture mesh. If considering the full substrate, a unique intermediate picture mesh induces even more missing particles, because a part of them were not counted between 0 and 80 μm, and also because the much larger Sentaurus mesh cannot well identify all the particle positions deeper in the substrate. The introduction of the second and large mesh for the intermediate picture improves the comparison with Geant4 as more particles are counted in the deep substrate. Therefore, this latter conversion method is more efficient and combines a good precision near the surface and better particle count in the substrate.

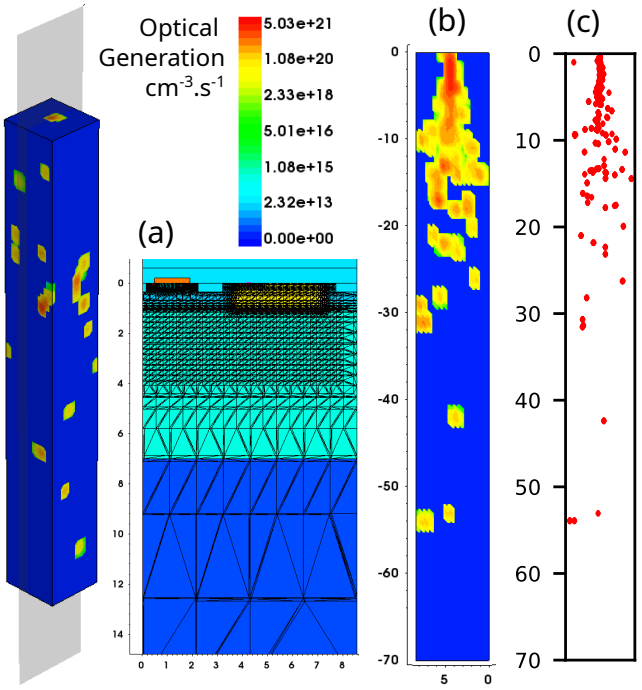

Fig. 6. On the left 3D TCAD optical generation after conversion of Geant4 particle positions, generated by 30 incoming electrons at 200 kV in one pixel. (a) is a cross-section of the doping concentration with the Sentaurus mesh, (b) is a cross-section of the optical generation and (c) is the comparison with the Geant4 output on the same field of view.

IV. Three Dimensional TCAD Simulations

The script presented above is adapted for three dimensional TCAD simulations. For this purpose, the third coordinate of each particle is read, and saved in the intermediate picture. A unique mesh is used in lateral dimensions and another fixed one is specified for the depth. These meshes are chosen to be in the same order of magnitude compared to the Sentaurus ones in the sensitive region. Therefore, in the example used in this paper, the lateral mesh is 500 nm and the vertical one is 1 μm, still smaller compared to the Sentaurus mesh in the deep substrate (Fig. 6 (a)). Then, the same interpolation function is used in Python, in order to build the optical generation file. The script is again fully executable in the Sentaurus workbench, and the Fig. 6 is showing the conversion of the same Geant4 particle distribution in a 3D Sentaurus optical generation with the following dimensions, $8 \times 8 \times 70$ μm^3. The particle beam enters in the substrate surface in the middle, and an optical generation of 10^{18} cm^{-3}.s^{-1} is specified.

The optical generation visible in the cross-section of the Fig. 6 (b) is comparable with the Geant4 output (c). While the position of the particles may look less accurate in the Sentaurus view due to the chosen mesh, the same distribution is visible. Depending on the particle distribution depth and shape, the lateral and vertical mesh of the intermediate picture

should be adapted in order to offer a good matching of the optical generation and the Geant4 simulation. This example demonstrates the correct behavior of the script converting the Geant4 simulation to a 3D optical generation file.

V. Discussion

The script presented in this work is fully integrable in the Sentaurus workbench and is quite efficient. Indeed, it reads only one time the whole list of particle positions given by the Monte Carlo simulation, and the longest part is the interpolation of each Sentaurus mesh points. As an example, the full Geant4 conversion of this study requires 30 s in 2D and 50 s in 3D on a Xeon 2.1 GHz processor.

However the script has some drawbacks. Firstly, one has to choose one or two meshes in 2D simulation and it may have some consequences on the resulting particle position precision, especially in the deep substrate where the Sentaurus mesh is generally large. However, the amount of charge is comparable to the Geant4 outputs, and the loss of precision in the deep substrate should be put in parallel with the fact that only charges in the vicinity of the photodiode are captured during one integration frame. Therefore, this issue should be acceptable. Secondly, this method cannot be used for the simulation of temporal particle propagation, and for measuring temporal tracks [15]. Only 2D or 3D fixed particle distributions can be simulated.

As a perspective, one improvement of the script could be the addition of a second vertical mesh in the 3D simulation for a better conversion of the particle position in the deep substrate.

VI. Conclusion

A new methodology is presented and allows for the integration of Geant4 particle distributions into the Sentaurus TCAD workbench. The method is fast, simple and only requires to chose the intermediate picture mesh for the conversion process, which could be based on 2 or 3 parameters. The proposed method is able to efficiently convert the particle positions if the intermediate picture mesh is kept in the same range of the Sentaurus one, and it has been demonstrated that the amount of particle found in Sentaurus are comparable with the Geant4 simulation. This methodology can be used for detector developments, and allows for powerful simulations of detectors with time dependent biases.

References

[1] B. D. A. Levin, "Direct detectors and their applications in electron microscopy for materials science," *Journal of Physics: Materials*, vol. 4, no. 4, p. 042005, jul 2021. [Online]. Available: https://dx.doi.org/10.1088/2515-7639/ac0ff9

[2] R. Ballabriga, J. Braach, E. Buschmann, M. Campbell, D. Dannheim, K. Dort, L. Huth, I. Kremastiotis, J. Kröger, L. Linssen, M. Munker, P. Schütze, W. Snoeys, S. Spannagel, and T. Vanat, "Transient monte carlo simulations for the optimisation and characterisation of monolithic silicon sensors," *Nuclear Instruments and Methods in Physics Research Section A: Accelerators, Spectrometers, Detectors and Associated Equipment*, vol. 1031, p. 166491, 2022. [Online]. Available: https://www.sciencedirect.com/science/article/pii/S0168900222001176

[3] D. Townsted, "Multimodality imaging of structure and function," *Physics in Medicine and Biology*, vol. 53, no. 4, pp. R1–R39, 2008.

[4] *Sentaurus Sdevice User Guide*, 2020th ed., Synopsys, September 2020.

[5] M. Raine, A. Valentin, M. Gaillardin, and P. Paillet, "Improved simulation of ion track structures using new geant4 models—impact on the modeling of advanced technologies response," *IEEE Transactions on Nuclear Science*, vol. 59, no. 6, pp. 2697–2703, 2012.

[6] H. Zhang, H. Liu, Z. Pan, S. Chen, and R. Chen, "Influence of ionisation track structure on 20 nm fdsoi transistor," *Microelectronics Reliability*, vol. 123, p. 114179, 2021. [Online]. Available: https://www.sciencedirect.com/science/article/pii/S0026271421001451

[7] M. Pocaterra, M. Ciappa, and P. Pfaeffli, "A unified model for tcad simulation of the charge generated in semiconductors by low-energy alpha particles and protons," *Microelectronics Reliability*, vol. 138, p. 114725, 2022, 33rd European Symposium on Reliability of Electron Devices, Failure Physics and Analysis. [Online]. Available: https://www.sciencedirect.com/science/article/pii/S0026271422002499

[8] D. Dannheim, K. Dort, D. Hynds, M. Munker, A. Nürnberg, W. Snoeys, and S. Spannagel, "Combining tcad and monte carlo methods to simulate cmos pixel sensors with a small collection electrode using the allpix2 framework," *Nuclear Instruments and Methods in Physics Research Section A: Accelerators, Spectrometers, Detectors and Associated Equipment*, vol. 964, p. 163784, 2020. [Online]. Available: https://www.sciencedirect.com/science/article/pii/S0168900220303181

[9] A. Loi and A. Contu, "Tcode: A new multithread simulator for silicon sensors in hep applications," in *2019 IEEE Nuclear Science Symposium and Medical Imaging Conference (NSS/MIC)*, 2019, pp. 1–4.

[10] O. Marcelot, D. Lambert, and C. Marcelot, "Integration of monte carlo transport simulations into a tcad workflow for electron detector developments," *IEEE Transactions on Nuclear Science*, vol. 72, no. 6, pp. 1849–1855, 2025.

[11] S. Agostinelli, , and al., "Geant4 a simulation toolkit," *Nuclear Instruments and Methods in Physics Research Section A: Accelerators, Spectrometers, Detectors and Associated Equipment*, vol. 506, no. 3, pp. 250–303, 2003. [Online]. Available: https://www.sciencedirect.com/science/article/pii/S0168900203013688

[12] J. Allison, , and al., "Geant4 developments and applications," *IEEE Transactions on Nuclear Science*, vol. 53, no. 1, pp. 270–278, 2006.

[13] ——, "Recent developments in geant4," *Nuclear Instruments and Methods in Physics Research Section A: Accelerators, Spectrometers, Detectors and Associated Equipment*, vol. 835, pp. 186–225, 2016. [Online]. Available: https://www.sciencedirect.com/science/article/pii/S0168900216306957

[14] M. D. Kelzenberg, "Silicon microwire photovoltaics," 2010. [Online]. Available: https://resolver.caltech.edu/CaltechTHESIS:06082010-074917811

[15] B. Bergmann, T. Billoud, P. Burian, C. Leroy, P. Mánek, L. Meduna, S. Pospíšil, and M. Suk, "Particle tracking and radiation field characterization with timepix3 in atlas," *Nuclear Instruments and Methods in Physics Research Section A: Accelerators, Spectrometers, Detectors and Associated Equipment*, vol. 978, p. 164401, 2020. [Online]. Available: https://www.sciencedirect.com/science/article/pii/S0168900220307981